Mon. Not. R. Astron. Soc. **314**, 263–272 (2000)

Adaptive optics near-infrared imaging of NGC 2992 – unveiling core structures related to radio figure-of-8 loops

Scott C. Chapman,[1]★† Simon L. Morris,[2] Almudena Alonso-Herrero[3] and Heino Falcke[4]

[1]*University of British Columbia, Department of Physics & Astronomy, Vancouver, BC, Canada V6T 1Z4*
[2]*Dominion Astrophysics Observatory, National Research Council of Canada, Victoria, BC, Canada V8X 4M6*
[3]*Steward Observatory, University of Arizona, Tucson, AZ 85721, USA*
[4]*Department of Astronomy, Max-Planck-Institut für Radioastronomie, Auf dem Hügel 69, D-53121 Bonn, Germany*

Accepted 1999 November 26. Received 1999 August 24; in original form 1999 March 1

ABSTRACT

We present near-infrared adaptive optics, Very Large Array (VLA) radio and *Hubble Space Telescope* (*HST*) optical imaging of the nearby Seyfert galaxy NGC 2992. Spiral structure and an extension to the west are traced down to the core region at the limiting resolution of our near-infrared images. A faint, diffuse loop of near-infrared and radio emission is also observed to the north, embedded within the prominent 2-arcsec radio loop previously observed to the north-west. Near-infrared colour maps and CO narrow-band imaging are then used to identify which regions may not be purely reddened stellar populations. Our new data provide evidence that the VLA radio-loop morphology in the shape of a figure of 8 represents two components superimposed: (1) outflow bubbles out of the plane of the disc, coincident with the extended emission-line region (EELR); (2) star formation along the spiral arm within the galaxy disc and through the dust lane. The near-infrared continuum emission associated with the outflowing radio bubbles suggests that the radio loops are driven by the active nucleus.

Key words: galaxies: active – galaxies: formation – galaxies: individual: NGC 2992 – galaxies: starburst – infrared: galaxies.

1 INTRODUCTION

NGC 2992 is an Sa galaxy seen almost edge-on with a nearby, likely interacting, companion (NGC 2993). It possesses an active Seyfert 1.9 nucleus. A large and prominent dust lane runs through the centre of the galaxy roughly north to south, splitting the nuclear region in two. Ulvestad & Wilson (1984) found that the radio structure of the nucleus of NGC 2992 has the shape of a 'figure of 8', with a maximum extent of about 550 pc, oriented out of the plane of the galactic disc (assumed distance 37.3 Mpc using the recession velocity relative to the Local Group of 1864 km s^{-1} (Ward et al. 1980) and $H_0 = 50\,\mathrm{km\,s^{-1}\,Mpc^{-1}}$, angular scale of 182 pc arcsec^{-1}). Most of of the 6-cm radio emission from the centre of the galaxy arises in the loops of the figure of 8 rather than in the nucleus.

There are several favoured models for such figure-of-8 radio emission. The loops could result from expanding gas bubbles that are seen preferentially as limb-brightened loops (Wehrle & Morris 1988). Such outflows may be associated with the active galactic nucleus (AGN) core. The continually diminishing X-ray emission has been interpreted as a dying active nucleus (Bassani et al. 1998), possibly because fuel is no longer being channelled down to an accretion disc region. However, this would not likely affect the appearance of the surrounding region at our resolution of ~20 pc, because even at outflow speeds close to c the time-scale is ~50 yr.

Alternatively, starburst-driven superwinds could result in expanding gas bubbles leading to such emission (Heckman, Armus & Miley 1990). Extended X-ray and Hα emission (Colbert et al. 1996; Colbert et al. 1998) perpendicular to the plane of the galaxy may be an indication for such a superwind. If the superwind were produced by an energetic burst of supernovae (SNe) in the past, the current radius of the loop would then imply that the SNe explosion occurred over 2.35×10^5 yr ago for a typical expansion velocity of 1000 km s^{-1} (Koo & McKee 1992; Tenorio-Tagle & Munoz-Tunon 1998).

A different model proposes toroidal magnetic fields, which result in loop-like synchrotron emission (Wehrle & Morris 1988). Here, strong differential rotation in the galactic nuclear disc builds up the magnetic field, which has some radial component, until an instability occurs, leading to an expanding magnetic arch. The field configuration upon expansion away from the nucleus is then a pair of loops. The synchrotron emission results when particles are accelerated to relativistic energies in the magnetic arches.

† Present address: Observatories of the Carnegie Institution of Washington, 813 Santa Barbara Street, Pasadena, CA 91101, USA.
★ E-mail: schapman@ociw.edu

We have observed NGC 2992 at high spatial resolution using the Adaptive Optics Bonnette (AOB) on the Canada–France–Hawaii Telescope (CFHT). This is part of a larger project to map the cores of nearby Seyfert galaxies in the near-infrared with adaptive optics in order to study core morphologies. Our new near-infrared imagery of NGC 2992 unveils emission features [dust obscured in optical wavelength *Hubble Space Telescope* (*HST*) imaging] that may be related to the Very Large Array (VLA) radio emission. This discovery allows a consistent model of the radio emission to be formulated, incorporating the larger scale bipolar morphology observed in Hα by Allen et al. (1999). In Section 2 we outline the observations and reductions. In Section 3 we present the results of our multiwavelength analysis. Finally, in Section 4, we discuss the implications of the observed morphologies for various models.

2 OBSERVATIONAL DETAILS

2.1 CFHT AOB imaging

Observations were obtained using the CFHT in 1997 March and 1998, with the AOB (Rigaut et al. 1998) feeding the Montreal Infrared Camera (MONICA) (in 1997) and Kilopixel Infra Red (KIR) (in 1998) near-infrared cameras (Nadeau et al. 1994). The AOB is based on the curvature wavefront sensing concept (Roddier et al. 1991), and uses a 19-zone bimorph mirror to correct for wavefront distortions. The MONICA detector is a Rockwell NICMOS3 array with 256×256 pixels and 0.034 arcsec pixel^{-1} sampling. The KIR camera replaced MONICA in early 1998, and uses the Hawaii $1\text{k} \times 1\text{k}$ pixel array with the same pixel sampling.

The core of this galaxy is sufficiently bright as a guiding source to enable near-diffraction-limited resolution under favourable natural seeing conditions. Adaptive optics (AO) correction is much more efficient in the near-infrared as a result of the $\lambda^{1.2}$ dependence of the Fried parameter, R_0, which characterizes the atmospheric coherence length. We obtained an *H*-band image with MONICA under good observing conditions [seeing full width at half-maximum (FWHM) <0.6 arcsec resulting in 0.15 arcsec resolution]. The *J*-, *H*-, *K*- and narrow-band CO images obtained with KIR had worse natural seeing than MONICA (>0.9) and the corrected point spread function (PSF) has an FWHM of $\sim$0.45 arcsec in *H*, *K* and CO, and $\sim$0.60 arcsec in *J*. When forming colour maps, images are always smoothed to the worse resolution of the pair of images in question.

As the field size is small (9×9 arcsec^2 for MONICA, 36×36 arcsec^2 for KIR), blank sky images were taken intermittently between science frames. On-source images were taken in a mosaic of four positions, alternately putting the galaxy core in each of the four quadrants of the array to account for bad pixels and image uniformity. Flux and PSF calibrations were performed using the UK Infrared Telescope (UKIRT) standard stars fs13 and fs25. Flat-field images were taken on the dome with the lamps turned on and off to account for the thermal glow of the telescope. Data reduction was performed in the standard way for near-infrared imaging: (i) bad pixel correction; (ii) sky subtraction, using a median-averaged sky estimate; (iii) flat-field correction; (iv) recentring and coaddition of the different exposures through cross-correlation techniques.

The continuum image for the vibrational transition CO(2–0) absorption ($\lambda_c = 2.296$ μm, $\Delta\lambda = 200$ Å) was estimated by fitting a line through several regions in the *J*, *H*, and *K* images with no apparent dust-lane structure. All images were convolved to 0.6 arcsec resolution before estimating the CO continuum image. This extrapolation was then sampled with a Gaussian of the same width as the CO narrow filter centred at 2.296 μm. This flux level was then used to normalize the *K*-band image for subtraction of the CO image, resulting in a [continuum − CO] index within the range typically observed (see for example Davidge & Courteau 1999 for results on M81 with the same CO filter used at CFHT). The above result was also checked against the following procedure. The outer regions of the image have typical early-spiral bulge colours (e.g. Glass & Moorwood 1985) and are likely to be relatively free of dust emission. By matching the *K*-band image in flux to the CO image near the outer edges of the field, we obtain a zero-point in the [continuum − CO] image. These two procedures were found to agree within 15 per cent.

Obtaining an accurate measure of the resulting PSF of the image with AO is problematic, because the atmospheric conditions are continually changing, and a stellar image taken before or after the science exposure will likely not resemble the PSF of the science frame. An accurate PSF must be temporally and spatially coincident with the actual region of interest in the field, because the PSF degrades away from the guiding source. Even when there is a star within the relatively small field of view of the near-infrared cameras used with AOB, the PSF is frequently quite different from the core of the active galaxy (guiding source). Attempts have been made to model the off-axis PSF in these cases with some success (Hutchings et al. 1998).

A technique has been developed to reconstruct a model PSF for the nuclear region of the galaxy using the adaptive optics modal control loop information obtained during the actual observations (Veran et al. 1998a,b). For the core brightness as seen by the wavefront sensor ($V = 16.5$) in the MONICA *H*-band image, simulations have shown that the reconstructed PSF should match the true PSF to an accuracy of approximately 10 per cent (Veran et al. 1998a). The factors degrading such a reconstruction are mostly the faintness and extension of the particular galaxy core, and superior results are obtained with brighter, point-like galaxy nuclei (or stars). The error in our reconstruction is mostly from the Strehl ratio and outer artefacts, with the FWHM being very close to that of the actual PSF.

The image is then deconvolved to the point at which the LUCY algorithm (Lucy 1974) converges ($\sim$25 iterations), using the model PSF as input. The LUCY deconvolution can create ringing artefacts around bright unresolved galaxy cores. However, the core of NGC 2992 is extended, while many of the structures surrounding the core are point-like. This is ideal for LUCY because the core region consists essentially of point sources superposed over a varying background. The algorithm was found to provide a believable deconvolution, with no new features appearing that were not in the original image at some level. The main benefit is the reduction of side lobes, and the seeing *pedestal* present with achieved Strehl ratios in the range 20–30 per cent. The estimated final resolution in the image is 0.12 arcsec, corresponding to 4 pixels.

2.2 Existing *HST* and UKIRT data

An archive *HST* F606W filter image was obtained with the WFPC2 camera in 1994 as part of a snapshot survey of nearby active galaxies (Malkan et al. 1998). The pixel scale with the PC camera is 0.044 arcsec pixel^{-1}. In order to compare this directly with our AOB image, we have interpolated and rebinned the image after rotating it to the proper orientation. The prescription

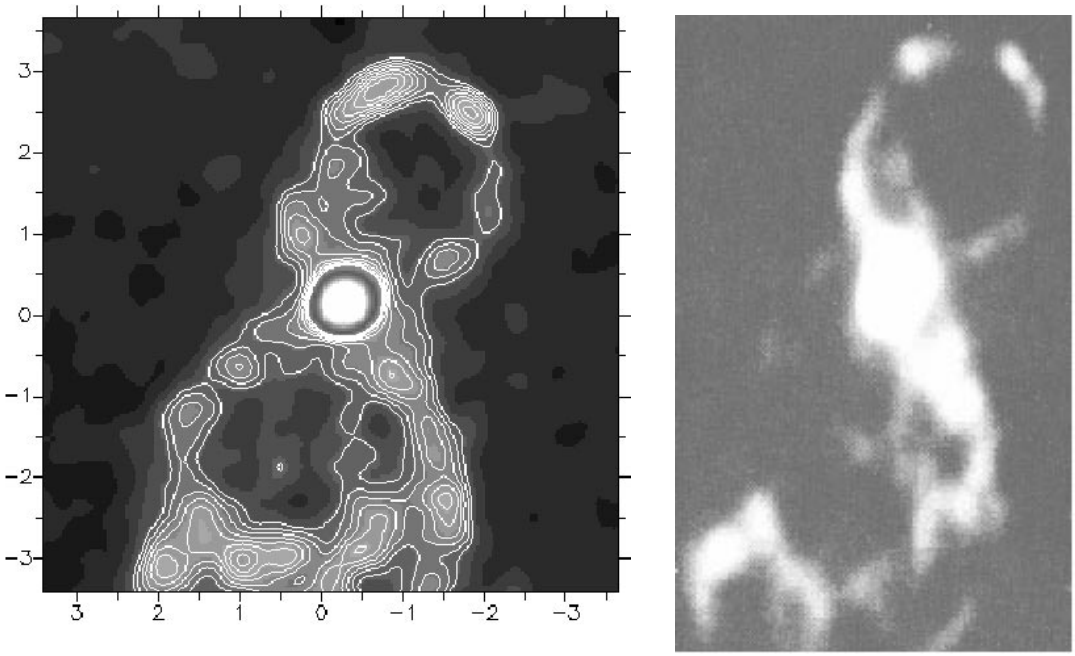

Figure 1. Left: 8.4-GHz image with contours overlaid (peak flux: 7.0 mJy; contour levels from 0.14 to 0.54 mJy, with intervals 0.045 mJy). Right: reproduction of the 5-GHz image (Wehrle & Morris 1988) (peak flux: 7.2 mJy). The peak flux at 1.5 GHz is 27.8 mJy (Ulvestad & Wilson 1984).

to calibrate the *HST* F606W image to the Johnson *V* band as outlined in Malkan, Gorjian & Tam (1998) is used for NGC 2992.

NGC 2992 was also observed at UKIRT in the near-infrared bands *J*, *H* and *K*. The plate scale is 0.29 arcsec pixel^{-1}. These data were originally presented by Alonso-Herrero et al. (1998).

2.3 VLA radio maps

A VLA image at 6 cm (5 GHz) was obtained in 1987 by A. Wehrle and is reproduced here with her permission (Fig. 1, right panel).

An image at 8.4 GHz (3.57 cm) was also obtained from the VLA archive (courtesy of H. Falcke) in C configuration, which resolves more clearly into knot-like structures (Fig. 1, left panel).

3 RESULTS

The morphology in the central region of NGC 2992 is a complicated superposition of various components, appearing most prominently in different wavelength regimes. An irregular-shaped patchy region dominates much of the western portion of the shorter wavelength images (especially the *R*-band – see Fig. 2 – and subsequent images). The fact that this region appears clearly as a deficit in the *R*-band image, and takes on a patchy morphology, is strong evidence for dust obscuration as the source of the colour gradient. The region is therefore most pronounced in long-baseline colour maps, such as $R-H$, with longer wavelengths being least affected by dust. Larger scale images of the galaxy reveal this feature as a dust-lane structure bisecting the core region (see Wehrle & Morris 1988). In Table 1, we list the various structural components in the core along with the figure that best highlights the feature.

3.1 The core region

In Fig. 2, we present the near-diffraction-limited *H*-band image of the central 7 arcsec of NGC 2992. The *HST* F606W (covering the $V+R$ band – hereafter called *R*) image is also depicted. The galaxy core is resolved in both the *H* and *R* filters, with a FWHM ~0.26 arcsec, corresponding to 47.2 pc. For the mediocre correction in the KIR *J* and *K* images, the core is essentially unresolved with FWHM 0.45 arcsec (*K*) and 0.6 arcsec (*J*). It is important to understand what percentage of the nuclear light may be emitted by an unresolved (AGN) component. We estimate the contribution to the extended galaxy core from the unresolved *H*-band component. Our model-constructed PSF (see Section 2 and Veran et al. 1998a) is a reasonable estimate of the true PSF for the diffraction-limited *H*-band image. We first produce a surface brightness profile of the galaxy using the IRAF task ELLIPSE, and another for the PSF. The PSF is then scaled to match the peak of the galaxy brightness. Both profiles are integrated out to a radial distance of 1 arcsec, with the result that the an unresolved component contributes at most 38 per cent in *H* in a 0.2-arcsec diameter aperture, and 17 per cent in a 0.5-arcsec aperture.

In Table 2 we present aperture photometry of the core region. The $V-H$ colour of the nucleus ($V-H=3.4$) is typical for a reddened stellar population (Glass & Moorwood 1985). Note that the deconvolved magnitudes agree with the raw data at an aperture radius of 3 arcsec. This is as expected, given that the deconvolution process restores flux to the central spike from the surrounding pedestal. This is encouraging despite the claims that deconvolved images may not be appropriate for photometry, because the non-linear algorithm does not necessarily conserve flux (Magain, Courbin & Sohy 1998). The disagreement with Alonso-Herrero et al. (1998) for the *H*-band apertures less than 3 arcsec in diameter is likely a result of the improved resolution of our image, coupled with our absolute errors of 4 per cent for the rms of calibration star measurements throughout the observing run.

The radio core spectrum is flat to within 5 per cent measured from our 8.4-GHz VLA image, in conjunction with archive 5-GHz and 1.5-GHz VLA measurements (mean of $\nu F_\nu = 3.4\times 10^{-16}$ erg s^{-1} – Wehrle & Morris 1988; Ulvestad et al. 1984).

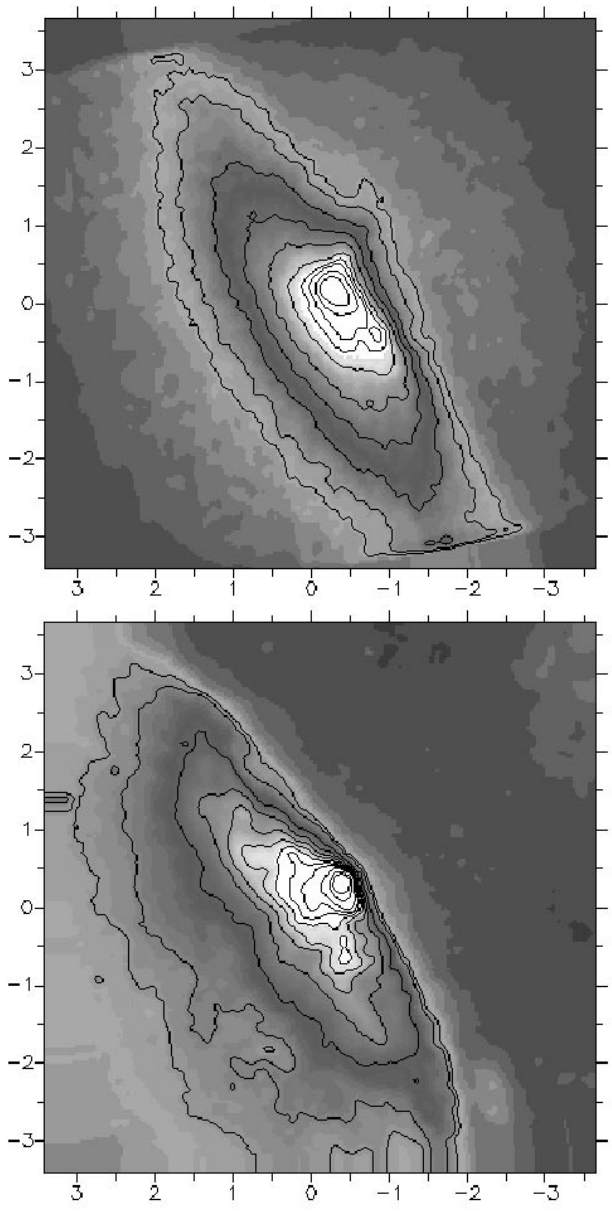

Figure 2. Upper panel: CFHT/AOB *H*-band image deconvolved with the LUCY algorithm. Lower panel: *HST* F606W ($R+V$ band) image – subsequently called *R* band. Contour levels are 1, 3, 5, 8, 11, 15, 20, 30, 50 and 80 per cent of peak ($H = 14.1$, F606W = 17.7).

This is indicative of the synchrotron emission arising in the AGN core dominating any possible synchrotron emission associated with supernovae at these wavelengths (Robson 1996).

Examination of the cores in both optical and near-infrared images (Figs 2, 3 and 4) reveals a bright point-like knot to the south, ~110 pc (0.6 arcsec) from the nucleus of the galaxy. A second knot to the south-west appears in the near-infrared only. An $[R-H]$ colour map is formed by first convolving the *HST* image with a Gaussian of width 0.12 arcsec to match the AOB resolution. The colour map (Fig. 5) reveals the south-western knot is almost 1 mag redder in $R-H$ than the southern knot, likely as a result of dust. The south-western knot is completely obscured in the *HST* image. We find that the colours in these regions ($V-H = 3.6$ to 4.2) are consistent with reddened stellar populations.

We perform aperture photometry on these knots in the *H* band and find apparent magnitudes between 16.0 and 16.5 in *H* depending on the aperture size used (the aperture measurements have relatively large error, because of their proximity to and overlap with the central AGN core). At the distance of NGC 2992, the absolute magnitudes lie between −15.3 and −14.8, comparable to the luminosities of stellar clusters detected in the interacting galaxy Arp 299, which have an average *H*-band absolute magnitude of $H = -15$ (Alonso-Herrero et al. 1998; Lai et al. 1998). Arp 220 (Scoville et al. 1998) also has compact stellar clusters of similar luminosities at 1.6 μm (*H* band). In the work of Scoville et al., merger remnants have been suggested as an explanation for such bright knots near the galaxy core (>10 per cent of the AGN peak for NGC 2992).

3.2 Spiral structure

The *H*- and *R*-band images (Fig. 2) show elongated isophotes to the south-west along the galaxy disc, and extending east from the nucleus. In the *R*-band case, the galaxy morphology is much more distorted because of the effects of dust. These extensions and distortions in the isophotes suggest structure underlying the elliptical symmetry of the disc within the central regions of the galaxy. We subtract a model image of the galaxy for both a large-scale *H*-band image (60 arcsec × 60 arcsec) and the AOB *H*-band image. The model is built from either elliptical fitted isophotes (Fig. 3) or a running median filter image with an FWHM of twice the resolution (Fig. 4). The elliptical isophote model has the advantage of highlighting structures deviating substantially from elliptical symmetry, while the median filtering tends to bring out fainter point-like structures. The profile in ellipticity (*E*) and position angle (PA) of the isophotal model shows that this region

Table 1. The structural components of NGC 2992.

Feature	Property	Flux	Size	Best figure	Location
resolved core	SF+AGN	$H = 13$	0.3 arcsec	All	
knots near core	SF	$H = 16$	unresolved	raw, smooth (2, 5)	S of nucleus
radio loops			2 arcsec	8.4 and 5 GHz (1)	NW,SE
near-infrared extension	non-stellar colours	$H = 15.3$	1 arcsec	model subtract (4)	NW
inner loop	SF		1 arcsec	$R-H$ (3)	N
diffuse radio	SF		1 arcsec	radio (1)	N
spiral arms	knots		3+ arcsec	model and smooth (4, 5)	NE–SW
assoc. radio?			3+ arcsec	radio (1)	NE–SW

has a substantial twist in both E and PA. In Fig. 3 (upper panel), the model-subtracted large-scale image displays what appears to be a spiral structure along the disc, as well as a ~3 arcsec extension to the west, also noted in Alonso-Herrero et al. (1998). Our new high-resolution images show that both the spiral structure

Table 2. Aperture magnitudes for the AOB H-band image, and *HST* F606W filter image corrected to V band.

Aperture diameter	H (deconvolved)	H (raw)	V (*HST*)
0.5 arcsec	14.08	14.50	17.46
1.0 arcsec	12.84	13.16	16.71
1.5 arcsec	12.29	12.50[a]	16.22
2.0 arcsec	11.96	12.08	16.17
3.0 arcsec	11.56	11.57[b]	16.14

[a] $H = 12.57$ from Alonso-Herrero et al. (1998).
[b] Magnitudes agree past the third Airy ring.

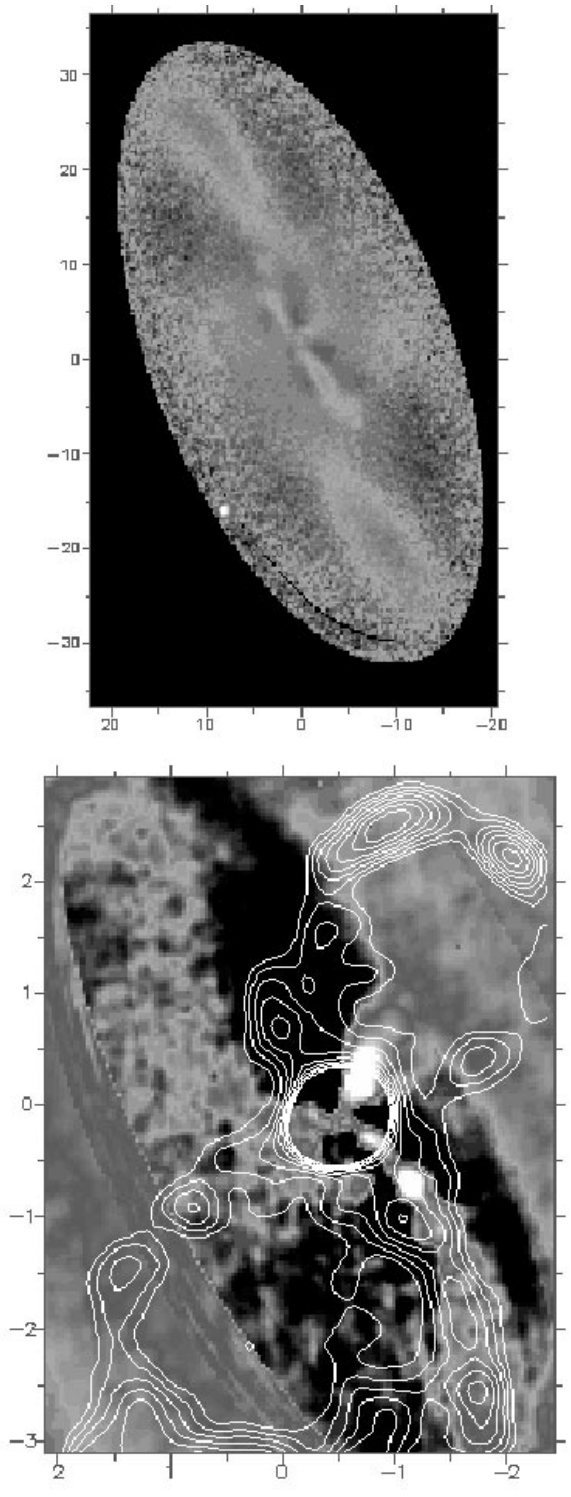

Figure 3. Upper: large-scale H-band UKIRT image with 0.29 arcsec pixels, elliptical isophote model subtracted. Lower: AOB H-band isophotal model-subtracted image of the central 6 arcsec × 4 arcsec of NGC 2992 with 8.4-GHz contours overlaid.

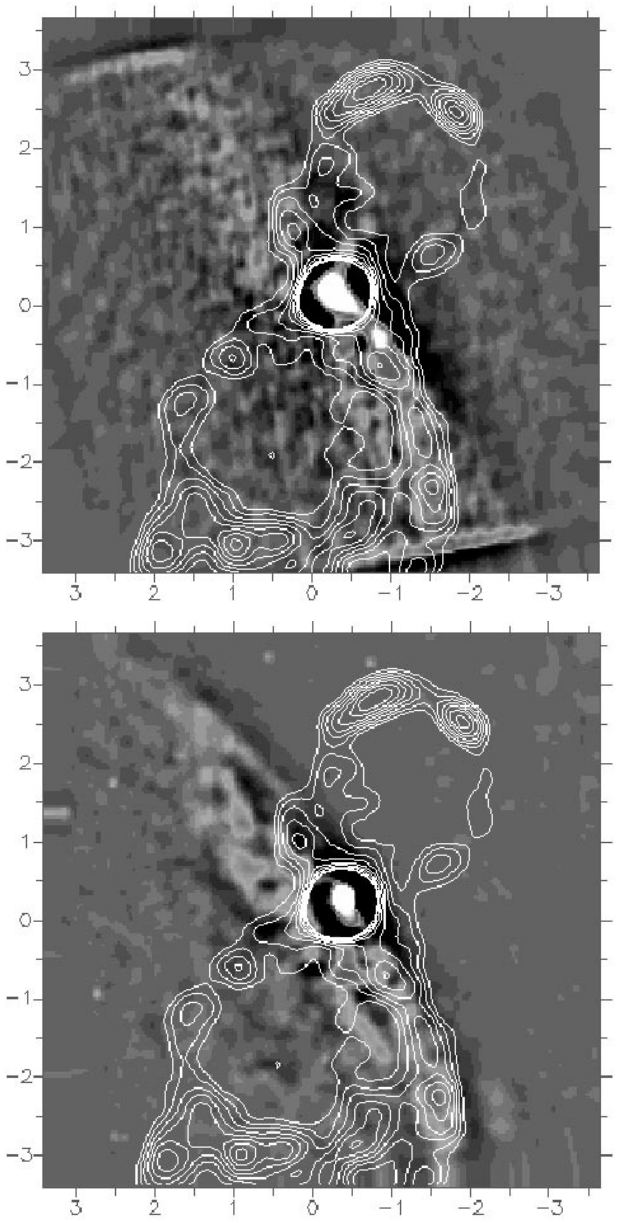

Figure 4. N2992 in H (upper) and R bands (lower), where a median-filtered image has been subtracted to remove the contribution of the low-order galaxy component. The 8.4-GHz radio contours have been overlaid.

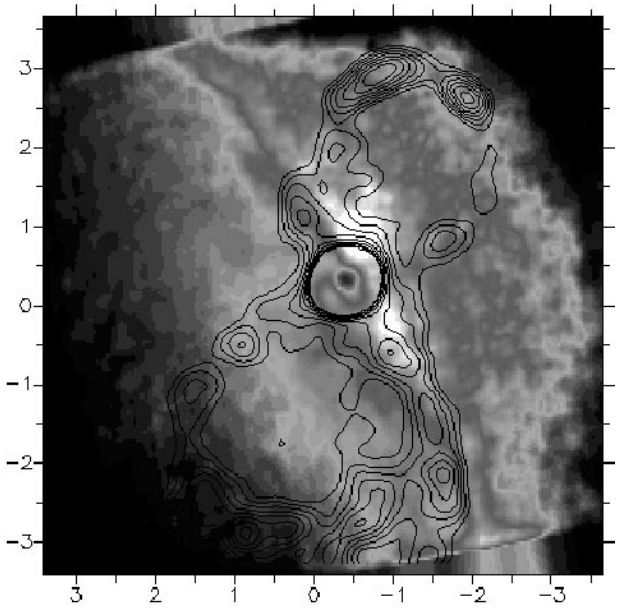

Figure 5. $R - H$ colour map with 8.4-GHz contours overlaid. The radio map core was centred on the near-infrared core. Brightest colours indicate the reddest regions with a maximum of $R - H = 4.8$, where the nucleus $R - H = 3.6$.

and western extension can be traced down to the very core. This latter extension will be taken up in the next section.

The image of the larger-scale galaxy shows a break in the spiral structures at ~7 arcsec radius. This may indicate nested structures that are kinematically distinct, as in the multilevel spiral arm structure observed with adaptive optics in NGC 5248 (Laine et al. 1998). Indeed, the knotty morphology of the spiral structures seen in the AOB and *HST* images of NGC 2992 are suggestive of star formation in spiral arms. The high inclination of NGC 2992 makes deprojection unreliable, and it is difficult to discern how these larger and smaller scale spiral structures relate. By the same measure, it is also difficult to know whether the isophotal twists in the core may be caused by a bar, a triaxial bulge seen in projection, or simply the effect of the spiral arms (Friedli et al. 1996).

In Figs 3 and 4, the 8.4-GHz radio contours are overlaid on the model-subtracted images. There is clearly some radio emission coincident with the southern spiral arm, which breaks up into a similar knotty morphology to the *H*-band model-subtracted image. Note especially that the strong near-infrared peak at the southern tip of the spiral arm has an associated peak in the radio, ~3 arcsec south and 2 arcsec west of the nucleus. We find the radio spectrum to be steeper along the spiral arm to the south than in the core, possibly indicative of star formation.

The prominent southern knots near the core, outlined in the previous section, clearly lie along the southern spiral arm. By comparing the brightest knots within the spiral arms in the optical and near-infrared images, it appears that the nuclei of the galaxy in the *H* and *R* bands, determined by centring on the cores, do not line up precisely. The knots in the southern spiral arm, revealed in the model-subtracted images, have similar geometric configurations in the two filters (*H* and *R*), but when these are superposed, there is a an (x, y) offset of (0.3, 0.15) arcsec between the nuclei, corresponding to a distance of ~70 pc. A true offset is possible, because of dust obscuration and/or extended unresolved starbursts [see for instance NGC 1068 (Alloin et al. 1998) for a similar case]. Given the much more distorted nuclear region in the *HST* *R*-band image compared with the *H* band, such a scenario is plausible. However, the spiral arm morphology may be slightly different in the two wavelengths, because of the effects of both dust and unresolved, blended structures. The difficulties in matching structures with slightly different morphologies in the outer galaxy lead us to register the images by centring on the galaxy nucleus.

3.3 Figure-of-8 loops

There is little sign of optical or near-infrared counterparts to the radio loops out past the disc of the galaxy, even in the *K* band, where the ability to see through the dust lane is greatest. However, as noted above, there is an extended feature to the north-west, observed as extended contours in the near-infrared (Fig. 2) and as a prominent feature in the model-subtracted near-infrared images (Fig. 3), extending ~1.5 arcsec before becoming more diffuse and mixing with the stellar emission on the western side of the dust lane. In the optical *HST* image (Figs 2b, 3b), there is no sign of this extended feature, likely because of the dust lane obscuration. This extension aligns with the mouth of the northern radio loop and appears to continue outwards into the loop, which is verified in the coarser resolution UKIRT image, where the signal-to-noise ratio allows the feature to be traced out further. This indicates that the source of the radio loop may be connected to this feature.

Fig. 5 shows that the extended feature is the reddest region in the central 7.0 arcsec of the galaxy, with an $R - H$ colour of 4.5. The lower resolution KIR images in *J*, *H*, *K* show that the colours in this region clearly stand out from the surrounding disc colours, possibly as non-stellar (in a 1-arcsec aperture, $J - H = 0.5$ and $H - K = 1.0$). These colours may be related to a highly reddened ($A_V > 5$) burst of stars, possibly with a nebular component. However, they are also consistent with a reddened continuum power-law emission (Glass & Moorwood 1985).

Artefacts associated with the AO correction have been shown to produce extensions to the PSF when guiding extended objects such as Seyfert nuclei (Chapman, Morris & Walker 1998). Although caution must therefore be taken in associating such a structure with a physical interpretation, we have compared our AOB *H*-band image with an *HST* NICMOS *K*-band image, and found the same extended isophotes to the west of the core.

3.4 Diffuse inner loop

The $R - H$ map (Fig. 5) shows extended red emission, which takes on a loop-like morphology extending north of the nucleus from the 1-arcsec to 2-arcsec declination offsets, an enhancement in *H* rather than a deficit in *R*. It does not appear to be associated with the spiral arm further to the east. In the median-filtered *H*-band image (Fig. 4), it is also possible to discern knotty features in a loop-like morphology; however, the emission lies deep within the region that is taken to be a dust lane, based on the obscuration of the *HST* optical imagery. No counterpart is seen in the model-subtracted *R* band (Fig. 4).

The 8.4-GHz radio contours superposed on the above figures (4 and 5) reveal a similar loop-like diffuse emission embedded within the larger, well-defined radio loop. The spectrum (from 5 to 8.4 GHz) is steeper here than in the core, consistent with star-forming regions. Buried star formation regions have been

identified in the dust lane crossing the nuclear region of Centaurus A (Schreier et al. 1996, 1998), using *HST* NICMOS images in the *H* band. The *J*, *H*, *K* colours in this region of NGC 2992 however are difficult to interpret in terms of the dust absorption gradient across the dust lane. It is not clear whether the structure has a true *loop* morphology, and it may be simply a result of the way the dust lane cuts through the core region. However, the coincidence of the radio emission suggests that the near-infrared excess may represent more than an artefact of dust absorption.

3.5 The CO map

The radial distribution of the CO index, (continuum-CO), is shown in Fig. 6, where the plotted values are azimuthal averages in 0.1-arcsec bins. Although the CO(2–0) filter used corresponds to the standard photometric index (2.296 μm centre, 200 Å width; Doyon et al. 1994), the subtracted continuum was extrapolated from the broad-band colours (see Section 2). There is then likely a systematic offset in absolute photometry, and we use caution in interpreting the CO magnitudes.

When $r < 1.5$ arcsec, the CO index strengthens implying much more CO absorption within the central 3 arcsec. The CO index depends on both the metallicity and the age of the stellar population (giants versus supergiants), and has been found to be difficult to model. If we assume that the metallicity is constant within the centre, then the variation may be an age effect. In general, the CO index increases as the starburst ages (Doyon et al. 1994; Vanzi, Alonso-Herrero & Rieke 1998). The NGC 2992 CO profile suggests that a somewhat younger population is present in a ring around the galaxy centre, while the stellar population in the very core would be slightly older than the surroundings. Given the rather poor resolution in these images (0.45 arcsec), we are unable to discern at what level the stellar population contributes within the resolved 50 pc core, evident in the *HST* *R*- and MONICA *H*-band images. However, it is clear that hot (∼1000 K) dust emission does not contribute significantly to the core region. The power-law tail of a strong hot dust continuum contribution in the *K* band would swamp the CO absorption signature, leading to a weakening CO index (less CO absorption). At larger distances the CO index shows a slight radial gradient, but this is not significant given the uncertainties in the background.

3.6 Characterizing the extinction

The effects of dust absorption become noticeably less with increasing wavelength in our images of NGC 2992. The *K*-band image has the most symmetrical appearance, with emission from the galaxy disc visible furthest into the dust lane. By referencing fiducial colours of expected stellar populations to the actual observed colours in NGC 2992, we can estimate the extinction caused by dust. The $H - K$ colour map is in general good for characterizing the extinction because it probes deeper within the dusty regions. However it has the problem that the *K* band may be contaminated by hot (1000 K) dust emission, resulting in possible overestimates of the extinction. Our CO narrow-band imaging confirms previous speculation from ground-based $J - K$ and $K - L$ colours (Alonso-Herrero et al. 1998) that hot dust is unlikely to contribute significantly.

We assume that the colour of a typical early-type bulge stellar population is $H - K = 0.2$ (Glass & Moorwood 1985), and that redder colours imply some degree of obscuration. Taking into account that the differential extinction between *H* and *K* is $A(H) = 0.175A(V)$ and $A(K) = 0.112A(V)$ (Rieke et al. 1985), we find

$$A(H-K) = -2.5\log\left[\frac{f(H)}{f(H_0)}\right] + 2.5\log\left[\frac{f(K)}{f(K_0)}\right],$$

where $f(K_0)/f(H_0)$ is the flux ratio corresponding to $H - K = 0.2$. Thus $A(V) = A(H-K)/0.063$ in magnitudes.

Such an analysis is only true for extinction to the stars. Other

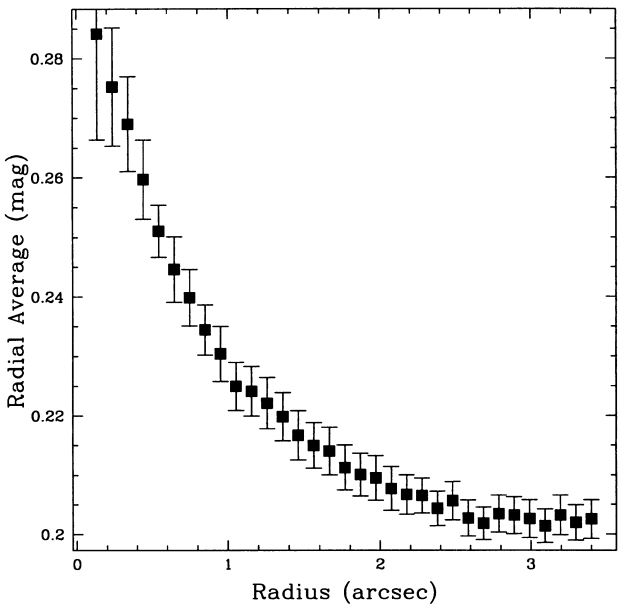

Figure 6. The CO index profile, (continuum − CO), near the centre of NGC 2992, where distances are measured with respect to the galaxy nucleus. The data points are azimuthal averages, and the error bars show the systematic errors introduced by uncertainties in the background.

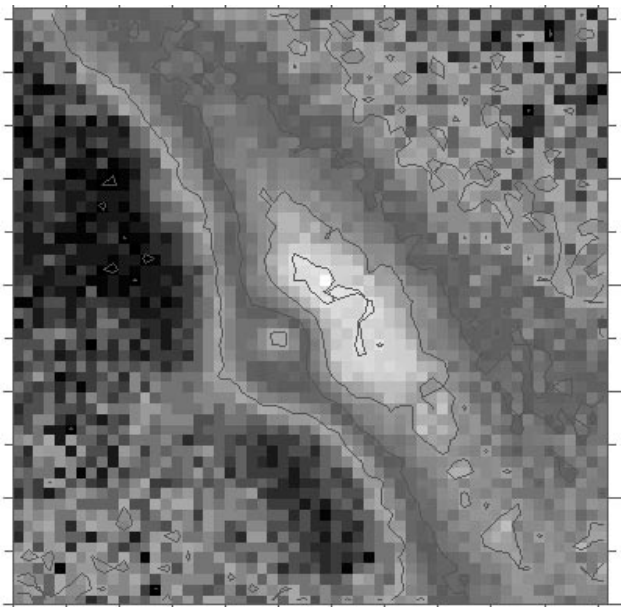

Figure 7. NGC 2992 $H - K$ map, central 5 arcsec, pixels binned to 0.1 arcsec. Contour levels are 2.6, 4.6, 6.6 and 8.6 mag of visual extinction $A(V)$. Images were smoothed with a 0.45-arcsec Gaussian before registration centred on the nucleus and forming the $H - K$ flux ratio map.

emission processes (power-law, emission-line gas, etc.) will skew the results. The $J - H$ and $H - K$ colours show that there are two regions that likely cannot be explained simply by reddened stellar colours. The first is within the dust lane, along the knotty spiral structure to the south and to the north along the diffuse loop described in Section 3.4. The colours here tend to be bluer in both $J - H$ and $H - K$, possibly indicative of nebular emission. The second is the extended region to the west of the nucleus, where the colours are far from the locus of normal stellar colours, and different from both the disc/bulge to the east and the rest of the colours within the dust lane.

The extinction map (Fig. 7) shows that if the central peak of emission is in fact caused mainly by a compact stellar core, then there is an optical extinction of $A(V) \sim 4$ mag. The $J - H/H - K$ colours of the nucleus are consistent with a reddened supergiant population. Taken at face value, the extinction map contours indicate $A(V)$ extinction from 2.6 to 8.6 mag with 2-mag intervals, although non-stellar emission likely over-reddens some of the circumnuclear regions, as discussed above. Using the $J - H$ map results in an extinction estimate that is lower, possibly as a result of the larger optical depth at shorter wavelengths.

4 DISCUSSION

We have combined the various structures observed in the different wavelength regimes and depicted them schematically in Fig. 8.

The radio loops lack any optical or near-infrared counterparts except along the galaxy disc axis. The bipolar outflows along the spin axis of the galaxy observed at larger scales in the optical (Allen et al. 1999) align along the same axis defined by the radio loops. These facts suggest that the actual figure-of-8 loops likely lie out of the galactic disc plane. However, the strong radio contours, emanating from the nucleus to the south-west, lie along the buried spiral arm within the disc. Also, the red $R - H$ loop to the north appears to be associated with the diffuse radio emission embedded within the larger radio loop.

Our hypothesis is then that the radio morphology consists of two components superimposed:

(1) the loops out of the plane of the disc;

(2) a component in the disc associated with the southern spiral arm, and a diffuse loop to the north. Starburst supernova remnants are the likely source of these radio components.

The appearance of the radio figure of 8 becomes more symmetrical if the galactic disc components (point 2 above) are subtracted, which supports such a superposition scenario.

The assumption of trailing large-scale spiral arms, in addition to the prominent dust lane likely lying in front of the bulge, imply that the north-west edge of the galaxy disc is closer to us. This scenario places the southern portion of the extended emission-line region (EELR) closer to us, with associated outflowing material (Allen et al. 1999). The southern radio loop would then also be closer to us, with the northern loop lying partially behind the dust lane. However, the larger scale spiral arms extending radially out past 30 arcsec appear to wind in the opposite orientation to the inner spiral observed in our high-resolution imagery. This either forces the inner spiral arms to be leading, or else they are trailing in counter-rotation, with the inner region kinematically distinct from the outer galaxy. The case is not clear from the velocity fields presented in Allen et al. (1999), which have low spatial resolution coupled with a complicated superposition of rotation and outflow components.

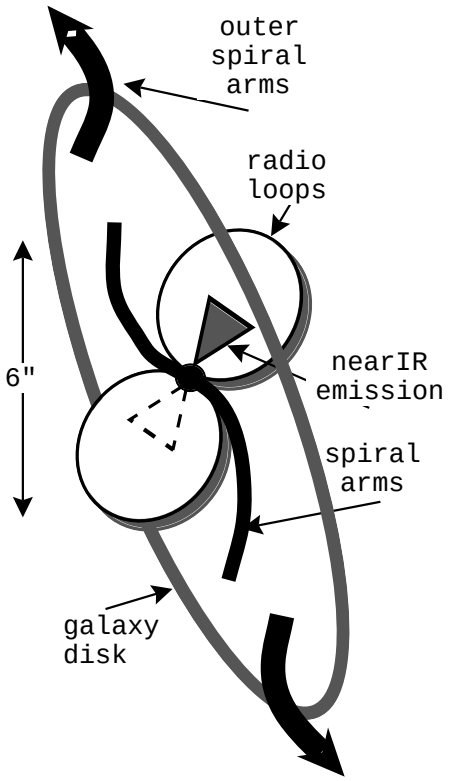

Figure 8. NGC 2992 cartoon displaying the hypothesized geometry in the central 7 arcsec (~1.3 kpc). The spiral arms lie within the galaxy disc (large grey ellipse), while the radio loops and possibly the near-infrared extended emission are projected out of the plane of the disc. The speculative extended emission inside the southern radio loop is depicted as a dashed cone. The larger scale spiral arms extending out past 30 arcsec radially appear to wind in the opposite orientation to the inner spiral. The assumption of trailing large-scale spiral arms, in addition to the prominent dust lane likely lying in front of the bulge, imply that the north-west edge of the disc is closer to us.

The near-infrared extended emission feature to the north-west gives the appearance of expanding into the northern radio loop, and the two emission features may be associated. The morphology and the rather extreme near-infrared colours suggest that an AGN-driven jet, possibly with some continuum component, could be directed into the radio loop. Hot dust present in an outflow is not ruled out for this feature either. This sort of near-infrared 'jet' may also exist towards the southern radio loop at a lower level.

4.1 Interpretation

As noted in the Introduction, there have been several models put forward for such figure-of-8 radio emission. The most convincing in light of our new near-infrared imaging is that the figure-of-8 loops result from expanding gas bubbles, which are seen preferentially as limb-brightened loops (Wehrle & Morris 1988). The northern loop may be related to the near-infrared extended emission feature to the north-west. Further evidence for the outflow picture exists in the form of soft X-ray emission extended perpendicular to the disc of the galaxy (Colbert et al. 1998), and Hα imagery clearly showing the location of an EELR (Colbert et al. 1996). These authors discuss two possible explanations for the extended X-ray emission: (1) an AGN-driven hot plasma and (2) a superwind from a compact starburst.

A galactic-scale superwind can be generated by either a compact starburst in the galaxy core or an AGN-driven outflow that thermalizes the ISM at some distance from the core (Colbert et al. 1996). In both cases the superwind would blow preferentially out of the galaxy plane where the pressure is lowest, as observed in NGC 253 (Unger et al. 1987). With the resolved galaxy core in our images, it is not clear to what extent dust absorption, hot dust emission, scattered AGN light or a compact stellar cluster contribute to the extended emission. The colours appear most consistent with reddened stellar light. Thus either picture could be consistent with our data, because a stellar cluster and AGN (optical emission lines, flat radio spectrum) are probably contributing to core emission processes. However, the larger scale EELR need not be aligned with the 2-arcsec diameter radio loops in the case of the AGN-driven source. The orientation of the EELR observed at larger scales (Allen et al. 1999) is in fact roughly aligned with the radio loops. For superwind models, the anisotropic EELR, seen in [O III] and Hα, is likely to be associated with the outflow regions. However, the superwind in itself does not yield a mechanism to produce continuum emission (Allen et al. 1999), and thus our near-infrared data may rule out this latter model.

If the near-infrared 'jet' is not actually related to the radio loops, the superwind model is still a plausible source of the loop emission. The CO index provides evidence for a substantial population gradient in the core. We consider the case where the radio loops are caused by an energetic burst of supernovae in the past. The luminosity of the stellar cluster must be at least three times that of the bubble, so the shock can reach a galactic scale height (Koo & McKee 1992; Tenorio-Tagle & Munoz-Tunon 1998). The stellar cluster luminosity is estimated from the *H*-band image. We determine the size of the 'hypothetical' stellar cluster to be 0.5 arcsec, with an absolute *H* magnitude of $-16.5 + M_{\rm AGN}$, where the AGN contribution is unknown and may be almost zero if the supermassive black hole is no longer being fuelled, as described in the Introduction (Bassani et al. 1998). The model PSF (Section 3.1) scaled to the peak of the extended core revealed that an unresolved AGN component could contribute at most 37 per cent to the emission within a 0.2-arcsec diameter aperture.

The second model outlined in the Introduction, with the toroidal magnetic fields causing the emission, is more difficult to explain in light of the near-infrared extension and knotty emission along the southern radio loop. The outflow-driven bubble model explains the currently available data much more naturally. In addition, a calculation of the magnetic energy in the loops from the 8.4-GHz VLA data (Werhle & Morris 1988; Falcke et al. 1998) makes it difficult to model consistently in this manner. Other problems with this model (Cameron 1985; Heyvaerts, Pudritz & Norman 1987; Wehrle & Morris 1988), associated with rotation time-scales and the lack of twisting of the radio/near-infrared loops, make it even less plausible.

5 CONCLUSIONS

We have presented adaptive optics near-infrared and radio images of NGC 2992, in conjunction with archive *HST* optical imagery. A spiral structure within the central 6 arcsec and a 1 arcsec extended feature are traced down to the core at the resolution of our images. We speculate that multiple radio components are superposed, which contribute to the observed figure-of-8 morphology in the VLA images: one associated with the spiral structure in the galaxy disc, and another flowing out of the galaxy plane.

Infrared and optical spectra at high spatial resolution will likely provide the means of determining whether the population gradients in the core of NGC 2992 are caused by changes in age and/or metallicity. Such spectral imagery will also permit the nature of the extended structures to be explored, shedding light on the possible connection to the radio loops.

Our current hypothesis concerning the radio loops involves an AGN outflow powering the loop, rather than a starburst superwind, as any near-infrared emission related to the jet would be unlikely in the latter case. NGC 2992 represents yet another example of star formation and AGN components both existing in the galaxy core (Storchi-Bergman et al. 1996). There is no obvious indication in our data of whether there is any connection between the two in evolutionary terms.

ACKNOWLEDGMENTS

We acknowledge the staff at CFHT and VLA for facilitating these observations. The CADC data base was invaluable in obtaining *HST* images.

REFERENCES

Allen M. G., Dopita M. A., Tsvetanov Z. I., Sutherland R. S., 1999, ApJ, 511, 686
Alloin D. et al., 1998, in Bonaccini D., ed., Proc. ESO/OSA, Vol. 56, Astronomy with Adaptive Optics. Sonthofen, Germany, p. 21
Alonso-Herrero A., Simpson C., Ward M. J., Wilson A. S., 1998, ApJ, 495, 196
Alonso-Herrero A., Rieke M. J., Rieke G. H., Scoville N. Z., 1999, ApJ, submitted
Bassani L., Dadina M., Maiolino R., Salvat M., Risalti G., Della Ceca R., Matt G., Zamorani G., 1999, ApJS, 121, 473
Cameron A. G. W., 1985, ApJ, 299, L83
Chapman S. C., Morris S. L., Walker G. A. H. W., 1998, in Bonaccini D., ed., Proc. ESO/OSA, Vol. 56, Astronomy with Adaptive Optics. Sonthofen, Germany, p. 73
Colbert E., Baum S., Gallimore S., O'Dea C., Lehnert M., Tsvetanov Z., Mulchaey J., Caganoff S., 1996, ApJS, 105, 75
Colbert E., Baum S., O'Dea C., Veilleux S., 1998, ApJ, 496, 786
Davidge T., Courteau S., 1999, AJ, 117, 2781
Doyon R., Wells M., Wright G. S., Joseph R. D., Nadeau D., James P., 1994, ApJ, 421, 101
Falcke H., Wilson A., Simpson C., 1998, ApJ, 502, 199
Friedli D., Wozniak H., Rieke M., Martinet L., Bratschi P., 1996, A&AS, 118, 461
Glass I., Moorwood A., 1985, MNRAS, 214, 429
Heckman T. M., Armus L., Miley G. K., 1990, ApJS, 74, 833
Heyvaerts J., Pudritz R. F., Norman C., 1987, in Backer D. C., ed., Proc. Symposium in Honor of C. H. Townes, The Galactic Center. AIP, New York
Hutchings J., Morris S. L., Crampton D., Steinbring E., 1998, PASP, 110, 374
Knapen J., Laine S., Yates J., Robinson A., Richards A., Doyon R., Nadeau D., 1997, ApJ, 490, L29
Koo D., McKee C., 1992, ApJ, 388, 93
Lai O., Rouan D., Rigaut F., Arsenault R., Gendron E., 1998, A&A, 334, 783
Laine S., Knapen J. H., Perez-Ramirez D., Doyon R., Nadeau D., 1998, MNRAS, 302, L33
Lucy L. B., 1974, AJ, 79, 745
Magain P., Courbin F., Sohy S., 1998, ApJ, 494, 472
Malkan M., Gorjian V., Tam R., 1998, ApJS, 117, 25
Nadeau D., Murphy D. C., Doyon R., Rowlands N., 1994, PASP, 106, 909
Rieke G. H., Lebofsky M. J., 1985, ApJ, 288, 618

Rigaut F. et al., 1998, PASP, 110, 152
Robson I., 1996, Active Galactic Nuclei. Wiley, West Sussex
Roddier F. J., Graves J. E., McKenna D., Northcott M. J., 1991, SPIE, 154, 248
Rouan D., Rigaut F., Alloin D., Doyon R., Lai O., Crampton D., Gendron E., Arsenault R., 1998, A&A, 339, 687
Scoville N. et al., 1998, ApJ, 493, L63
Schreier E., Capetti A., Macchetto D., Sparks W., Ford H., 1996, ApJ, 459, 535
Schreier E. et al., 1998, ApJ, 499, L143
Storchi-Bergmann T., Rodriguez-Ardila A., Schmitt H. R., Wilson A., Baldwin J., 1996, ApJ, 472, 83
Tenorio-Tagle G., Munoz-Tunon C., 1998, MNRAS, 293, 299
Ulvestad J. S., Wilson A., 1984, ApJ, 285, 439
Unger S. W., Pedlar A., Axon D. J., Whittle M., Meurs E. J. A., Ward M. J., 1987, MNRAS, 228, 671
Vanzi L., Alonso-Herrero A., Rieke G. H., 1998, ApJ, 504, 93
Veran J. P., Rigaut F., Maitre H., Rouan D., 1998a, J. Opt. Soc. Am., 14, 11
Veran J. P., Rigaut F., Maitre H., 1998b, in Bonaccini D., Tyson R., eds, Proc. SPIE, Vol. 3353, Optical Science. Engineering and Instrumentation. SPIE, Bellingham, p. 426
Ward M., Penston M., Blades J., Turtle A., 1980, MNRAS, 193, 563
Wehrle A. E., Morris M., 1988, AJ, 95, 1689

This paper has been typeset from a TEX/LATEX file prepared by the author.